An initial-value problem for testing numerical models of the global shallow-water equations

By JOSEPH GALEWSKY*, RICHARD K. SCOTT and LORENZO M. POLVANI, *Department of Applied Physics and Applied Mathematics, Columbia University, New York, NY 10027, USA*

ABSTRACT

We present an initial-value problem for testing numerical models of the global shallow-water equations. This new test case is designed to address some of the difficulties that have recently been uncovered in the canonical test case suite of Williamson et al. The new test case is simple to set up, yet able to generate a complex and realistic flow. The initial condition consists of an analytically specified, balanced, barotropically unstable, mid-latitude jet, to which a simple perturbation is added to initiate the instability. The evolution is comprised of an early adjustment phase dominated by fast, gravity wave dynamics, and a later development characterized by the slow, nearly balanced roll-up of the vorticity field associated with the initial jet.

We compute solutions to this problem with a spectral transform model to numerical convergence, in the sense that we refine the spatial and temporal resolution until no changes can be visually detected in global contour plots of the solution fields. We also quantify the convergence with standard norms. We validate these solutions by recomputing them with a different model, and show that the solutions thus obtained converge to those of the original model. This new test is intended to serve as a complement to the Williamson et al. suite, and should be of particular interest in that it involves the formation of complicated dynamical features similar to those that arise in numerical weather prediction and climate models.

1. Introduction

The shallow-water equations are important for the study of the dynamics of large-scale atmospheric flows, as well as for the development of new numerical schemes that are applied to more complex models. In order to evaluate numerical schemes for the solution of the shallow-water equations, Williamson et al. (1992, hereafter W92), proposed a suite of standard tests, and offered reference solutions to those tests obtained with a pseudo-spectral scheme (Jakob-Chien et al., 1995, hereafter J95).

While the W92 tests have proved to be a useful reference point in recent years, their widespread use has revealed a number of serious problems that severely limit their practical utility. Test cases 1–4 have simple analytical solutions and are useful for debugging and establishing some key characteristics of the numerical scheme being tested. However, the flows associated with these tests are completely idealized and thus largely unrepresentative of typical atmospheric conditions. Test cases 5–7, in contrast, do attempt to capture a variety of different atmospheric flows. Recent findings, however, have revealed some unexpected subtleties which render them less useful than originally thought.

Specifically, test case 5 involves flow over an isolated mountain, but the mountain topography as defined in W92 is not a differentiable function: this is obviously problematic. Spectral models, for instance, are likely to exhibit ringing phenomena as the resolution is increased, as reported in J95. Moreover, the mountain is added impulsively on to a initially balanced flow; needless to say, this generates a solution that is very difficult to capture numerically, as it necessitates extremely small time-steps during the early stages of evolution during which the flow adjusts to the presence of the mountain by generating gravity waves (Todd Ringler, private communication).

Test case 6, an initial wavenumber-4 Rossby–Haurwitz wave, has also turned out to be much more subtle than originally suspected. As Thuburn and Li (2000) have recently shown, this initial condition generates complex small-scale features in the vorticity field as a consequence of a triad instability of the initial flow (Baines, 1976). Surprisingly enough, truncation errors are sufficient to instigate the instability. Furthermore, the details of the small features are highly dependent on the diffusive nature of the scheme used to compute the solution, and are thus very difficult to reproduce. Again, these difficulties were not mentioned in the reference solutions offered by J95.

Finally, test case 7 has proven to be rather unpopular, as it requires the downloading of the initial fields, and involves some

---
*Corresponding author.
e-mail: jg2282@columbia.edu

cumbersome steps (e.g. interpolations) that make it somewhat impractical. Similarly, comparison with reference solutions is unnecessarily cumbersome.

We here propose a new test case that specifically addresses the difficulties we have just discussed. The new test case uses simple, analytical functions for the initial condition, and is thus easily implemented. In addition, from these simple initial conditions, the new test case is able to generate complex dynamics that are representative of atmospheric flows. The new test case is nothing but a barotropically unstable zonal flow, to which a simple perturbation is added to induce the instability.

One benefit of the new initial condition is that it naturally captures both of the intrinsically different physical motions exhibited by fluids that obey the shallow-water equations: the fast, divergent gravity wave motion, and the slow, nearly balanced vorticity dynamics. As a consequence of the initial perturbation, gravity waves are generated by an adjustment process and propagate around the globe within a few hours, while complex vortical dynamics, including the roll-up of the initial flow into vortices and formation of tight vorticity gradients, develop over a few days. The distinction of these two time-scales is important, and none of the W92 test cases appears to have addressed this issue.

The paper proceeds as follows. We first present the expressions that define the initial conditions for the new test case. We next compute numerical solutions with a pseudo-spectral scheme, for both the early-time unbalanced adjustment process and the later-time vorticity-dominated barotropic instability. The numerical solutions are computed at progressively higher spatial and temporal resolution until global contour plots of all prognostic fields (at specific times) cease to change with further refinement. While this may not appear to be a highly sophisticated procedure, we suggest that is an important, simple and practical first step that ought to be performed prior to computation of any derived quantity. We submit that some of the problems with the W92 test suite could have been avoided if this had been done consistently. We then compute a variety of norms, along the lines of those proposed in W92, to provide more quantitative insight into our numerical solutions. Finally, we validate our solutions by recomputing them with a different numerical model. We conclude with a brief summary of the suggested steps for the new test case.

2. Initial condition

In vector form, the viscous shallow-water equations can be written as

$$\frac{\mathrm{d}V}{\mathrm{d}t} = -f\boldsymbol{k} \times \boldsymbol{V} - g\nabla h + \nu\nabla^2\boldsymbol{V}$$

$$\frac{\mathrm{d}h}{\mathrm{d}t} = -h\nabla\cdot\boldsymbol{V} + \nu\nabla^2 h \tag{1}$$

where $\mathrm{d}/\mathrm{d}t$ designates material derivative, the prognostic variables are $\boldsymbol{V} = \boldsymbol{i}u + \boldsymbol{j}v$, the velocity vector tangent to the spherical

surface (where $\boldsymbol{i}$ and $\boldsymbol{j}$ are the unit vectors in the eastward and northward directions and u and v are the corresponding velocity components), and h is the thickness of the fluid layer. The other notation is standard: $f \equiv 2\Omega\sin\phi$ is the Coriolis parameter (ϕ denotes latitude), Ω is the angular velocity of the Earth, g is the acceleration due to gravity, and ν is the diffusion coefficient. The numerical values for the constants we have adopted for this test case are $\Omega = 7.292 \times 10^{-5}$ s^{-1} and $g = 9.80616$ m s^{-1}.

Ideally, one might want to use inviscid equations for a test case. As we will demonstrate, for realistic flows this is not a viable option due to the extremely fast generation of small-scale features in geophysical flows. As the diffusion greatly controls the evolution of the flow, it is necessary to explicitly specify what diffusion is being used in order to generate reproducible results. For maximum simplicity, we have opted for a standard diffusion operator.

The initial condition for the new test case consists of a basic zonal flow, representing a typical mid-latitude tropospheric jet, with a correspondingly balanced height field, plus a small unbalanced perturbation to the height field; the perturbation is used to induce the development of barotropic instability. Both the basic flow and the initial perturbation are analytically specified, allowing the complete initial condition to be easily reproduced.

For the basic flow, the zonal velocity component u is a function of latitude

$$u(\phi) = \begin{cases} 0 & \text{for} \quad \phi \leq \phi_0 \\ \dfrac{u_{\max}}{e_{\mathrm{n}}}\exp\left[\dfrac{1}{(\phi-\phi_0)(\phi-\phi_1)}\right] & \text{for} \quad \phi_0 < \phi < \phi_1 \\ 0 & \text{for} \quad \theta \geq \phi_1 \end{cases} \tag{2}$$

where $u_{\max}$ is the maximum zonal velocity, ϕ_1 is the latitude of the northern boundary of the jet in radians, ϕ_0 is the latitude of the southern boundary of the jet in radians, and e_{n} is a non-dimensional parameter that normalizes the magnitude of the jet to a value of $u_{\max}$ at the jet's mid-point. The constants are chosen as follows: $u_{\max} = 80$ m s^{-1}, $\phi_0 = \pi/7$, $\phi_1 = \pi/2 - \phi_0$, $e_{\mathrm{n}} = \exp[-4/(\phi_1 - \phi_0)^2]$, for which the jet's mid-point is located at $\phi = \pi/4$.

This function has several useful features that make it particularly suitable for use in this test case. The function is explicitly defined to be zero outside the region of interest, ensuring that there are no discontinuities at the poles (which is required to ensure finite vorticity at the poles). The function is also infinitely differentiable, a characteristic that is desirable for many numerical schemes. Commonly used functions, such as a hyperbolic secant, a truncated cosine or a Gaussian function, either do not go to zero at the poles or are not infinitely differentiable.

With the initial basic zonal flow given by eq. (2), the height h is obtained by numerically integrating the balance equation

$$gh(\phi) = gh_0 - \int^{\phi} au(\phi')\left[f + \frac{\tan(\phi')}{a}u(\phi')\right]\mathrm{d}\phi', \tag{3}$$

where a is the radius of the Earth (we use $a = 6.37122 \times 10^6$ m for this test case) and the constant h_0 is chosen so that the global mean layer depth is equal to 10 km. While the choice of the numerical scheme for the evaluation of the integral above is left to the reader, we note that h can be computed to machine precision using standard Gaussian quadratures with something of the order of a hundred points, pole-to-pole.

In order to initiate the barotropic instability, the basic flow just described is perturbed by adding a localized bump to the balanced height field, of the form

$$h'(\lambda, \phi) = \hat{h} \cos(\phi) e^{-(\lambda/\alpha)^2} e^{-[(\phi_2 - \phi)/\beta]^2}$$
$$\text{for} \quad -\pi < \lambda < \pi, \tag{4}$$

where λ is longitude (in radians), $\phi_2 = \pi/4$, $\alpha = 1/3$, $\beta = 1/15$ and $\hat{h} = 120$ m. Note that the Gaussian functions here are multiplied by the cosine of the latitude in order to force the perturbation to be zero at the poles. Figure 1 shows latitudinal profiles of the initial zonal flow and the corresponding balanced height field, together with a contour map of the perturbation height field.

Before presenting our results, we present a note about error analysis. We broadly follow the global error measures proposed in W92, which we reproduce here for convenience. For a field ξ, we define $I(\xi)$ to be the discrete approximation to the global integral of ξ

$$I(\xi) = \frac{1}{4\pi} \int_0^{2\pi} \int_{-\pi/2}^{\pi/2} \xi(\lambda, \phi) \cos \phi \, d\phi \, d\lambda, \tag{5}$$

which we calculate using Gaussian quadrature. Next, the l_2 norm of a field ξ is defined by

$$|\xi|_2 = \sqrt{I(\xi^2)}. \tag{6}$$

Finally, the normalized l_2 relative error for ξ is defined by

$$l_2(\xi) \equiv \frac{\left\{ I\left[(\xi(\lambda, \theta) - \xi_{\text{ref}}(\lambda, \theta))^2\right] \right\}^{1/2}}{\left\{ I\left[\xi_{\text{ref}}(\lambda, \theta)^2\right] \right\}^{1/2}}, \tag{7}$$

where ξ_{ref} is a reference field. Ideally, the reference field would come from the known analytical solution; when an analytical solution is unavailable, as in the case presented here, a high-resolution numerical solution is used instead.
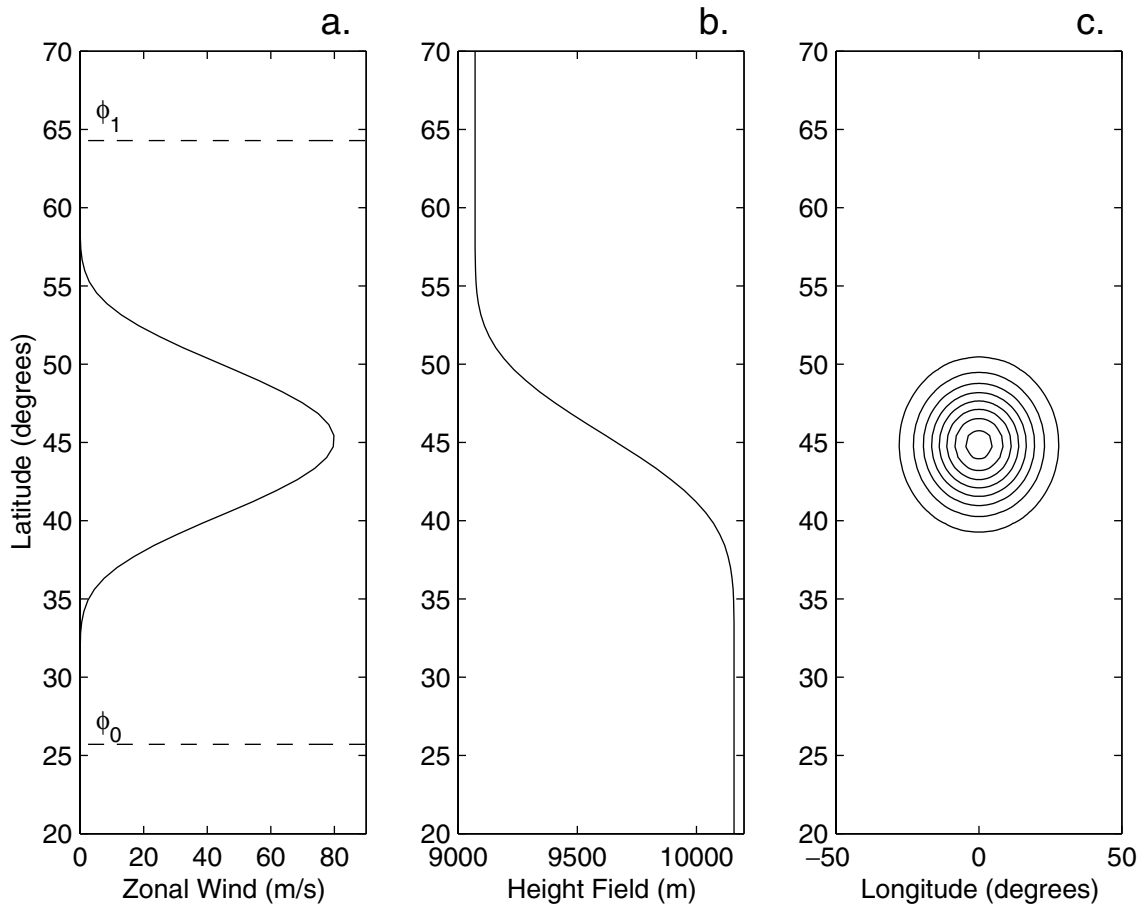

Fig 1. The initial conditions for the new test case. (a) The zonal wind, as defined in eq. (2); (b) the corresponding, balanced height field, calculated using eq. (3); (c) the height field perturbation, as defined in eq. (4), with a contour interval of 10 m; the outermost contour is at 10 m.

3. Numerical results

Having discussed how to set up the initial conditions for the new test case, we now present numerical solutions computed with the Geophysical Fluid Dynamics Laboratory (GFDL) FMS Shallow-Water Model (FMS-SWM; using the 'Havana' release version). This model solves the shallow-water equations using a spectral-transform method with a Robert–Asselin-filtered semi-implicit leapfrog scheme for time integration. The value of the Robert–Asselin filter for all runs presented here is 0.001. The results are calculated at four triangular spectral truncations of increasing resolution, T42, T85, T170 and T341, each using a time-step of 30 s, unless otherwise noted. The l_2 relative errors for the T42, T85 and T170 resolutions are calculated using the T341 resolution as the reference solution. We begin by considering the inviscid equations; hence $\nu = 0$ in eq. (1) unless stated otherwise.

As a preliminary step, we integrate the shallow-water equations for 120 h with the zonal jet and the unperturbed, balanced height field as initial conditions. This step is useful to ensure that the unperturbed zonal flow is properly balanced. In our FMS-SWM solutions, all fields remained identical to the initial ones to machine precision for the entire 120 h.

Beyond checking the balance of the initial unperturbed state, this step is in some sense trivial for a spectral model because the spectral method has no means of generating non-zonal components from an initially zonal flow. In general, however, this step is important because it tests the ability of a numerical scheme to maintain a steady zonal jet with a steep vorticity gradient. The maintenance of a zonal jet is potentially problematic for some numerical schemes, such as low-order methods on non-isotropic grids. We present no further specific details of this step here, because several of the W92 test cases are specifically designed to address this issue.

3.1. Adjustment problem

As already mentioned, when the perturbation is added to the balanced height field, the dynamics evolve on two distinct time-scales: a fast one associated with the rapidly developing gravity waves, and a slower one associated with the vortical dynamics. We first examine early-time results related to the gravity wave dynamics.

In Fig. 2, we show snapshots of the height and divergence fields from the FMS-SWM solution at T341 at 2, 4 and 6 h. Notice how the waves radiate from the center of the initial perturbation (marked by an asterisk in Fig. 2), as expected in a classic Rossby adjustment problem. To avoid imposing unnecessary map projections on future users of this test, the results are plotted on a simple longitude–latitude rectangle. Also, the initial balanced height field is subtracted from the instantaneous height field before plotting, to bring out the location of the wave front.

It is important to note that the solution presented in Fig. 2 is numerically converged, in the sense that the figure will not change if the temporal or spatial resolution is further refined. In fact, the contour plots for the T170 solution (not shown) are identical to those in Fig. 2; this is not surprising given the scale of the features generated at these early times. Similarly, the time-step was progressively halved to obtain convergence; we found that a time-step of 30 s was sufficient at T341 resolution. In addition, we have produced identical results using explicit time-stepping, as should be expected given the small time-step used here (Hoskins and Simmons, 1975). Again, these are not shown as the contours are completely superposed.

For completeness, we illustrate the convergence with spatial resolution by examining the time evolution of l_2 relative errors of the FMS-SWM solutions in Fig. 3, with the T341 solution used as the reference. In general, the l_2 relative errors in the divergence field are two orders of magnitude greater than those in the height field, and the T170 solutions are about one order of magnitude more accurate than the T42 solutions.

3.2. Barotropic instability

We now turn to the vortical dynamics, which develop on a longer time-scale than the gravity wave results just described. Figure 4 shows the inviscid evolution of the vorticity field (ζ) over 6 d, computed with FMS-SWM at T341 resolution, illustrating the development of the barotropic instability. There are several points to be made about this figure. First, note how the initially unstable vorticity field rolls up into a number of vortices, with the rolled-up region progressively moving eastward (typical of convective instabilities), in a manner characteristic of atmospheric flows.

The second important point is that, as the instability matures, the vorticity develops extremely tight gradients, which are clearly visible in the later frames. It is well known that the formation of these tight gradients is a generic feature of nearly two-dimensional flows. The small-scale noise apparent in Fig. 4 is due to the fact that, in the inviscid case, our spectral model is unable to capture the very small scales (with the accompanying tight gradients) that are being generated by the instability, even at this relatively high resolution.

As a consequence, the solution in Fig. 4 is not numerically converged, in the sense that plots of the solutions at lower resolutions (T42, T85 and T170) look very different from the ones presented there. In fact, they look much noisier, and we have not reproduced them here because that noise is an artifact of the spectral method, and is thus of no general interest and is not reproducible with other numerical schemes.

The accompanying l_2 relative errors are shown in Fig. 5 for the zonal wind, the vorticity and vorticity gradient, computed for the T42, T85 and T170 solutions relative to the T341 solution. Note first that $l_2(u)$ is essentially flat for the T85 and T170 solutions.
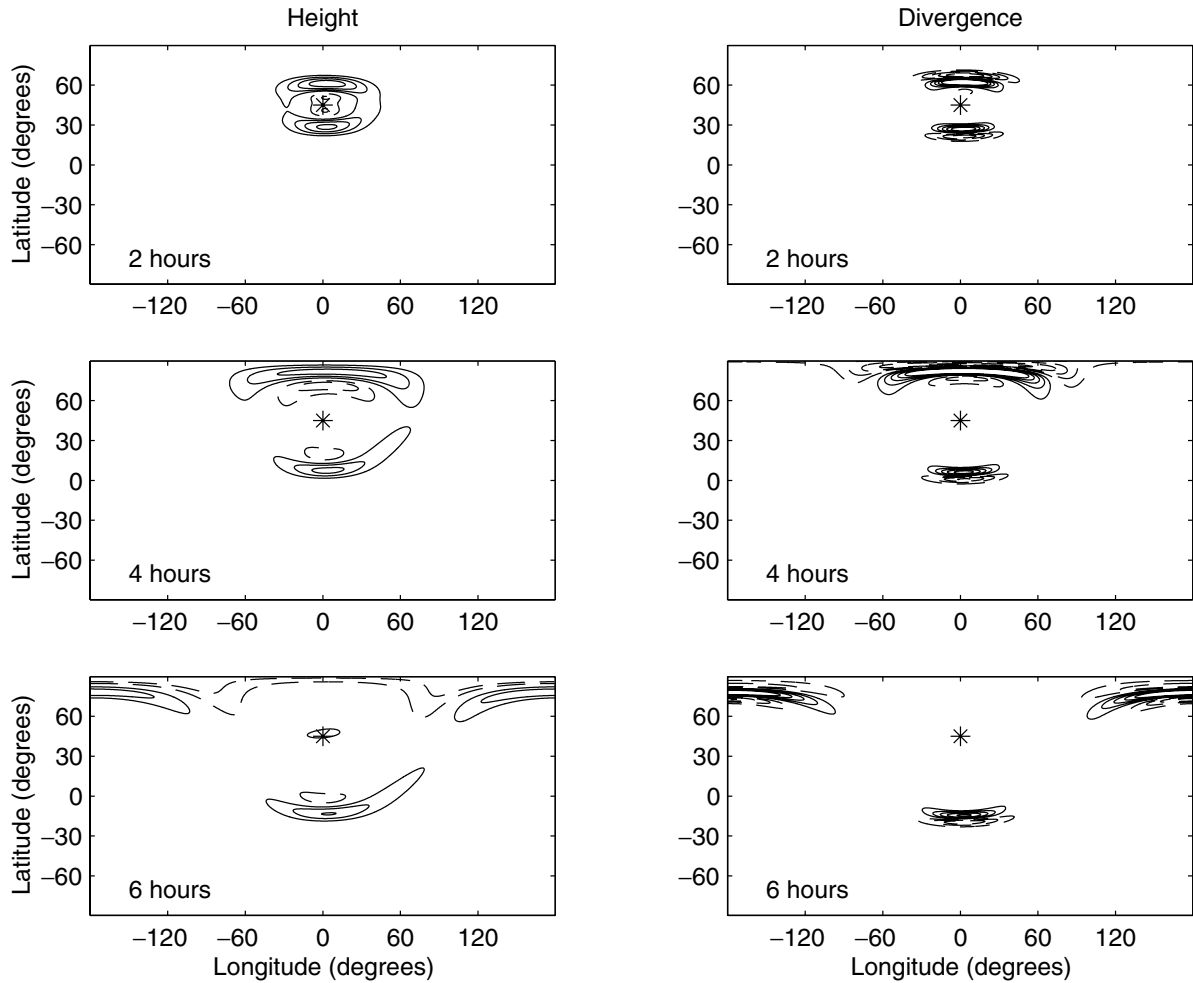
Height

Divergence

Fig 2. The numerically converged height and divergence fields during the adjustment process, computed with the FMS-SWM at T341 with a 30-s time-step. The height displayed here is the instantaneous h minus the balanced, unperturbed, initial height calculated in eq. (3); the contour interval is 4 m. For the divergence field, the contour interval is 4×10^{-7} s^{-1}. Negative contours are dashed. The asterisk in each plot indicates the center of the original perturbation.

From this, one is incapable of detecting the presence of the large numerical artifacts immediately apparent in Fig. 4. Similarly, $l_2(\zeta)$ and $l_2(\nabla\zeta)$, although growing after day 4, obscure how much noise is actually present in the vorticity field. The reason for the discrepancy rests in the fact that the global integral in the computation of l_2 is a smoothing operation. In view of this, we believe that it is important to produce global contour plots of the actual prognostic fields, prior to calculating derived quantities (e.g. norms).

In Fig. 5d, we plot the time evolution of the maximum value of the vorticity gradient for the four solutions (T42, T85, T170 and T341). This plot suggests no evidence of convergence, and opens the possibility that even larger values would result at higher resolutions. Because shocks can develop in the rotating shallow-water system (Kuo and Polvani, 1997), we have no guarantee that a finite-time singularity, for instance, would not spontaneously

appear from our initial conditions. However, it should be quite clear that the kind of singularity that might form here is not a traditional shock, in the sense of the height becoming double valued; the initial perturbation in the height field is only of the order of 1% of the mean height and, in addition, waves in rotating shallow water are dispersive.

It may be possible to establish the existence of well-behaved inviscid solutions by computing at extremely high resolutions. In fact, we have attempted to do this in two ways. First, we have computed solutions with our initial condition for 10 d using the contour-advective semi-Lagrangian (CASL) scheme (Dritschel et al., 1999) without any contour surgery, and the integration (not shown) is able to proceed without problems. As the CASL scheme is highly non-diffusive, this computation suggests that a smooth inviscid solution exists. Secondly, we have computed spectral solutions with progressively smaller hyperdiffusion up
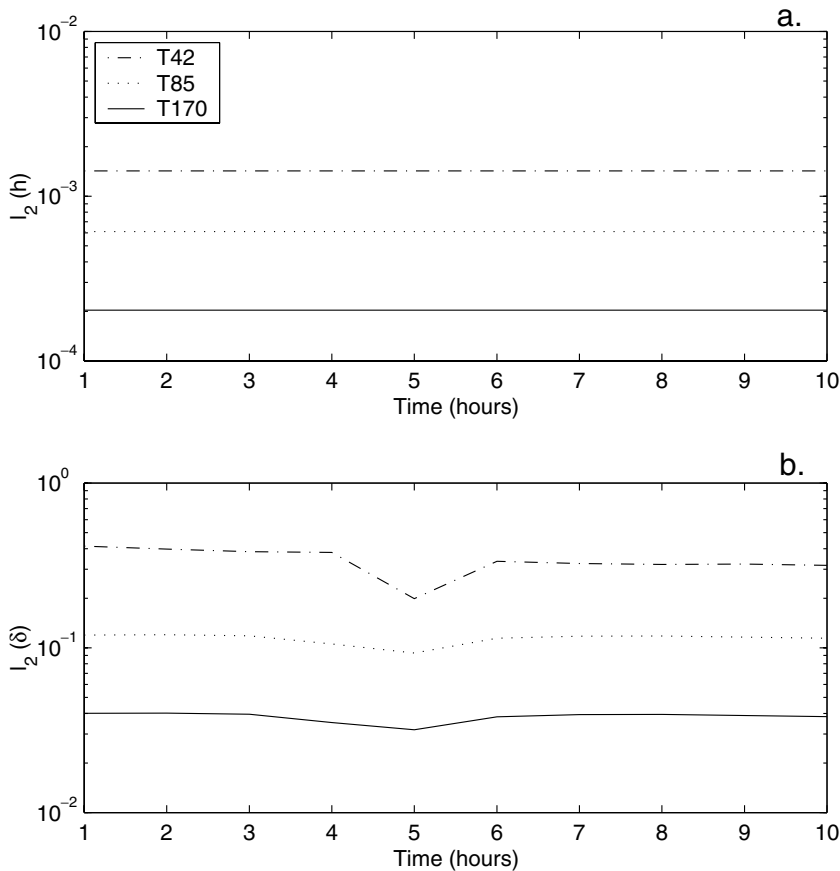
to T684 (not shown) and have seen no evidence of singularity. This suggests that, if one could increase the resolution sufficiently, one might be able to compute smooth solutions with no hyperdiffusion at all. However, the resolution needed to compute smooth, converged, inviscid solutions at day 6 is likely to be extremely high, and this would make for a highly impractical test case.

So, what is one to do? One possibility would be to stop the integrations well before the formation of tight vorticity gradients, say around day 3 in our case. At that stage, however, the flow is only starting to become unstable (cf. day 4 in Fig. 4) and is thus not representative of the kind of complexity of realistic atmospheric flows.

The other possibility, of course, is to control the complexity of the flow by introducing an explicit diffusion. This is what is done in practice in the majority of climate models, and is therefore the way we now proceed. For simplicity and easy reproducibility, we have chosen to use ordinary $\nu \nabla^2$ diffusion, as in eq. (1).

A variety of other diffusion operators could have been chosen, e.g. a $\nu \nabla^4$ hyperdiffusion operator as in the National Center for Atmospheric Research (NCAR) Community Climate Model (Kiehl et al., 1996), and a range of values for ν could be applied in each case. With spectral models, it is customary to choose the value of ν to be as small as possible for a given resolution, and to progressively decrease that value as the resolution is increased. In the present context, however, we are interested in the numerical solution to a specific set of partial differential equations (PDEs), calculated at different resolutions. If the value of ν were changed as the resolution was increased, we would effectively be changing the PDEs themselves, and hence would not be able to attain numerical convergence, in the sense described above, and thus to compare model results. For this reason, all of the solutions presented in this section are computed using $\nu = 1.0 \times 10^5$ m^2 s^{-1}, irrespective of resolution. This value was chosen to ensure that the numerical solutions converge at a resolution close to T85 at day 6 for the initial conditions of our test case.

Figure 6 shows the evolution of the vorticity field for the case with explicit diffusion, computed at T341 resolution. Note that the presence of diffusion controls the development of tight vorticity gradients, and generally produces a much smoother solution than in the inviscid case. At 144 h, the inviscid case (Fig. 4) has developed extremely tight vorticity gradients, while the gradients in the diffusive case (Fig. 6) are much weaker.

The key point of this figure, however, is that it is numerically converged, in the sense that this figure is identical to the one at T170 (not shown), and even nearly identical to the one at T85. Hence no further refinement of the spatial discretization is needed for convergence. Similarly, we tested that
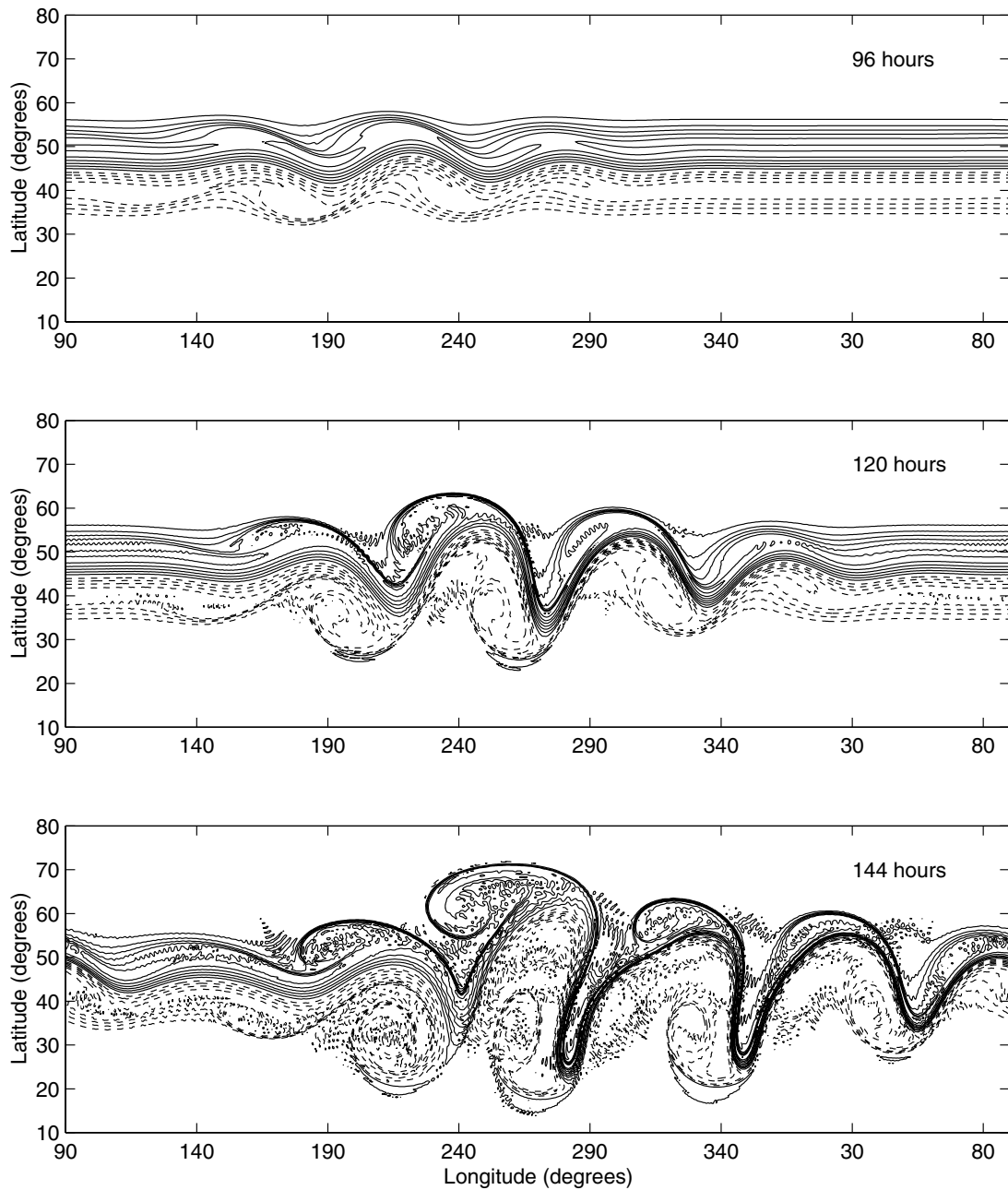
Fig 4. The time evolution of the vorticity field for the inviscid initial-value problem, computed with the FMS-SWM at a resolution of T341 with a 30-s time-step. The contour interval is 2×10^{-5} s^{-1}. Negative contours are dashed. The zero contour is not shown.

time-steps shorter than 30 s make no difference in the contour plots.

For completeness, the l_2 relative errors for the diffusive case are shown in Figs. 7a–c. The impact of diffusion is particularly evident in the plots of maximum vorticity gradient (Fig. 7d). Note how the initial vorticity gradient is eroded by the diffusion even before significant growth of the barotropic instability. Because of this, both the T170 and T85 models are able to maintain the same maximum vorticity gradient as the T341 model.

Finally, we mention that the solutions to the diffusive problem remain smooth even for relatively long times (10 d or longer), with none of the spectral ringing seen in the inviscid case.

4. Computational validation

Having demonstrated that the solution of the shallow-water equations from our simple initial condition produces realistically complex features on two distinct time-scales, and that one
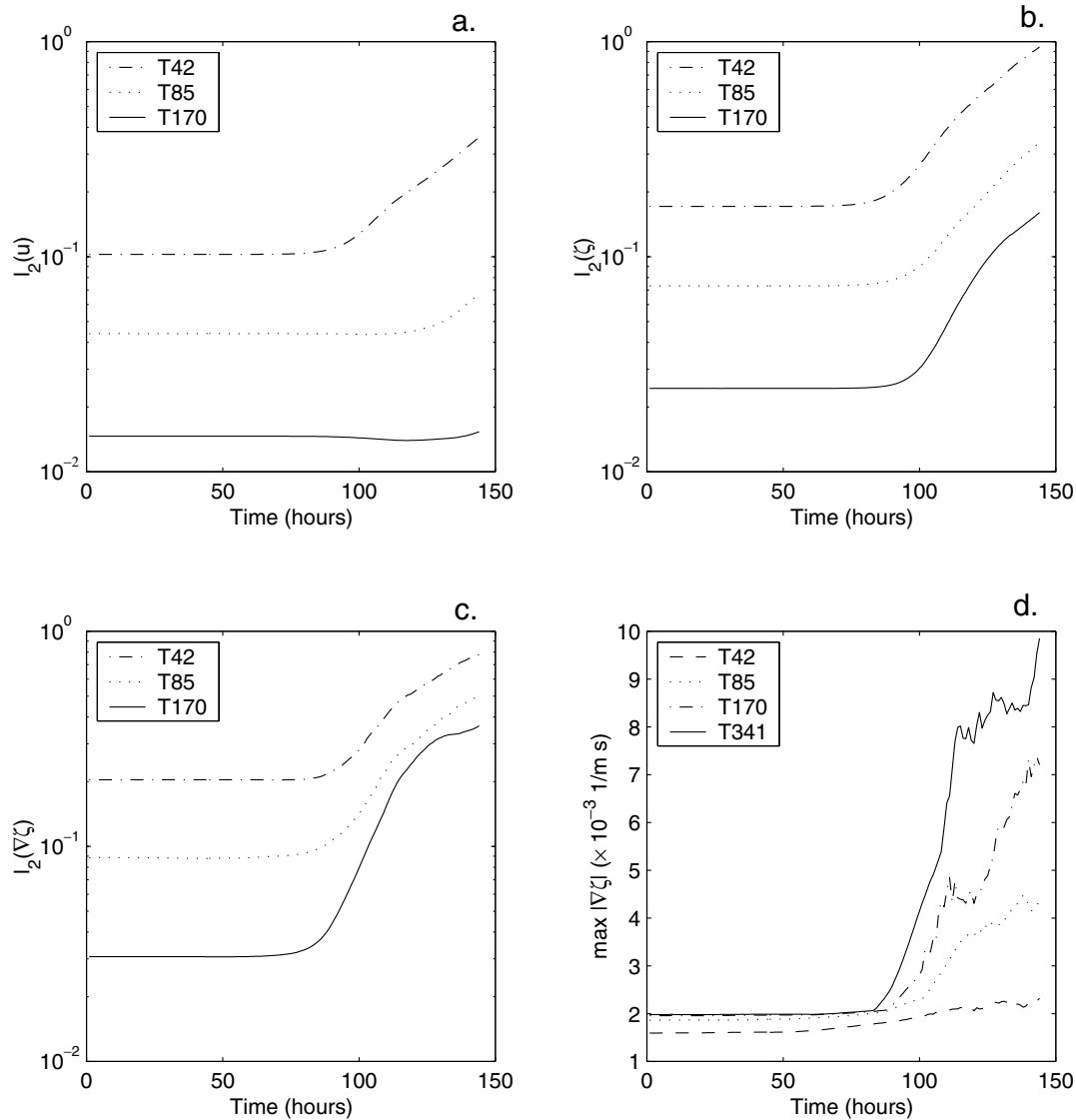
Fig 5. Semilog plots of the l_2 relative errors for (a) the zonal wind u, (b) the vorticity ζ, and (c) the magnitude of the vorticity gradient $\nabla\zeta$, for the inviscid test case, calculated relative to the T341 solution. (d) The maximum vorticity gradient as a function of time for T42, T85, T170 and T341 models.

numerical model (the FMS-SWM) is able to compute converged solutions in the sense that global contour maps of the prognostic fields become insensitive to resolution once a sufficiently fine grid is used to capture all the scales produced within a finite time interval, we now address the question of whether the converged solutions we have presented above are reproducible by other models.

To the best of our understanding, because we are explicitly controlling (through a diffusion term) the smallest scales that are generated by the instability over a finite (and relatively short) time interval, the solutions of the shallow-water equations have no means to develop singularities and are thus well behaved, as the solutions of the previous section suggest. Because of this,

we see no reason why the solutions presented above should not be reproducible by other numerical models. In fact, even for the primitive equations, it has been shown that two different numerical schemes can converge to an identical solution, in a similar test case (Polvani et al., 2004), provided that an explicit diffusion scheme is specified.

It is conceivable, however, that the FMS-SWM code we have used above may not be entirely free from programming errors. To eliminate this possibility, we have recomputed the solutions with another spectral transform model, the NCAR BOB Shallow-Water Model (Rivier et al., 2002; Scott et al., 2004). This code was developed completely independently from the FMS-SWM, uses different transform routines, and was compiled and executed
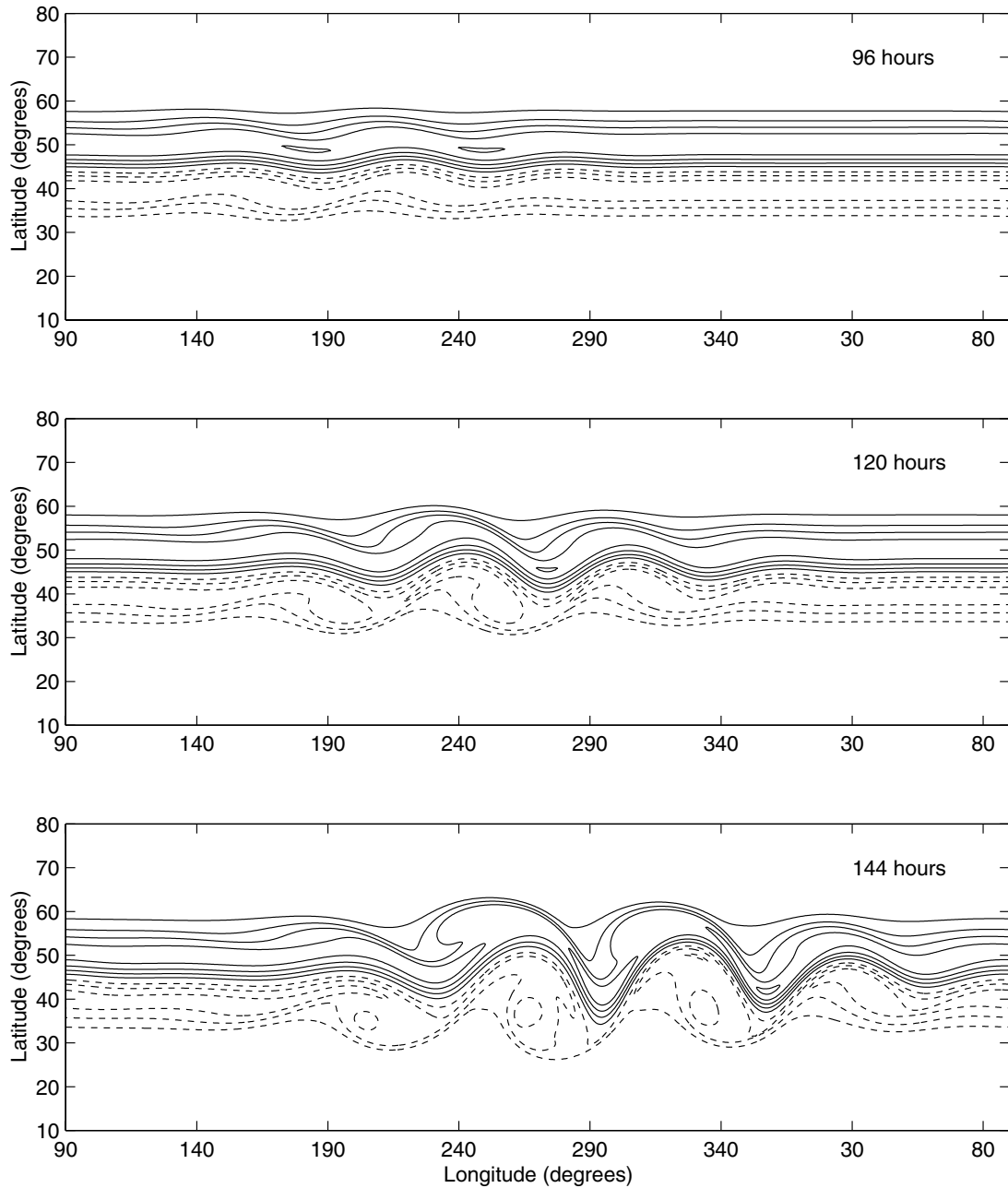
Fig 6. As in Fig. 4, but for the solutions with explicit diffusion. The diffusion coefficient $\nu = 1.0 \times 10^5 \text{ m}^2 \text{ s}^{-1}$.

on a different platform. We recognize that it would have been superior to use a different numerical scheme as well, but for the purposes of checking for programming errors any model should suffice.

In Fig. 8, illustrating the vorticity field at 144 h, we show how the BOB-SWM solutions (solid lines) converge (in the sense mentioned above) to the FMS-SWM T341 solution (dashed line) as the resolution is increased. Past T85, it is nearly impossible to distinguish the two sets of curves. We have produced a similar convergence plot of the height and divergence fields for the

adjustment problem (at 4 h) but, because the contours are superposed, we do not include it here.

Of course, one can be quantitative and demonstrate convergence by computing relative error norms. For the sake of completeness, in Fig. 9 we plot the l_2 relative error for both the divergence field (δ) during the adjustment stage (4 h) and the vorticity field (ζ) during the roll-up (144 h). The l_2 relative error is here computed, as a function of the BOB-SWM resolution, using the FMS-SWM solution at T341 as the reference solution. Confirming the visual impression of convergence illustrated in
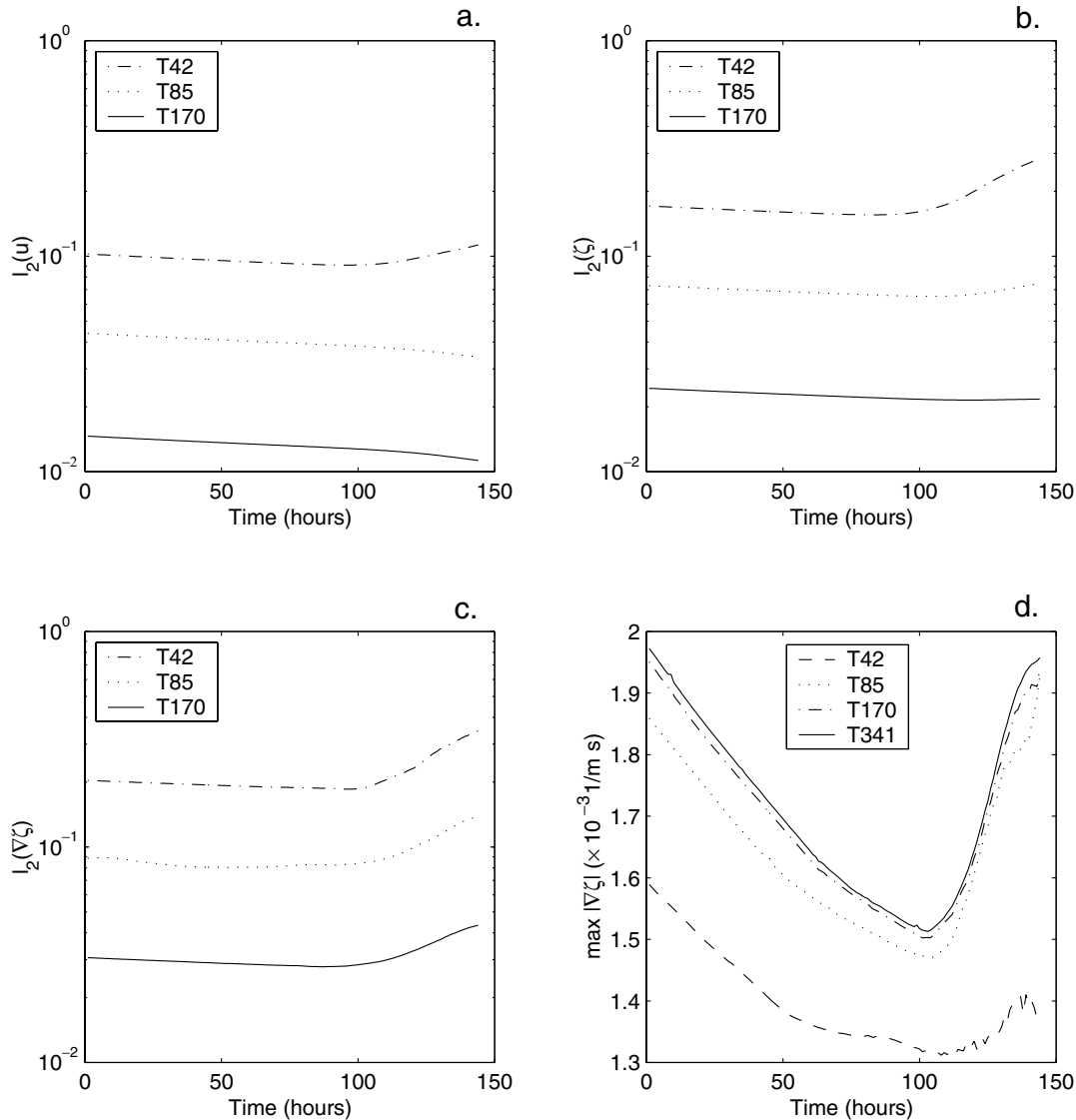
Fig 7. As in Fig. 5, but for the solutions with explicit diffusion.

Fig. 8, the l_2 relative error demonstrates that the BOB-SWM solutions are in fact converging to the FMS-SWM solutions. This gives us confidence that the solutions presented in this paper should be reproducible by any numerical scheme.

5. Conclusion

We have constructed easily implemented initial conditions for the shallow-water equations that generate a complex and realistic flow within a short integration period. We have computed numerically converged solutions using a spectral transform model, and we have validated them by reproducing them with a different numerical model. We offer this test case as a useful complement to the W92 test suite.

For testing numerical models, we suggest that the new test case be performed as described below. We emphasize that, at each stage, the spatial and temporal resolution should be refined until global contour plots of the solutions fields do not change with further refinement. We consider this to be an important and very practical, if only qualitative, first step. We see little point in calculating more sophisticated diagnostics if the truncation errors are large enough to be seen in simple contour plots.

First, initialize the model with the zonal wind as given in eq. (2) and the corresponding balanced height field (eq. 3), but with no explicit perturbation, and integrate for at least several days with no diffusion ($\nu = 0$). Note that the initial flow, while steady, is dynamically unstable. At very coarse resolutions,
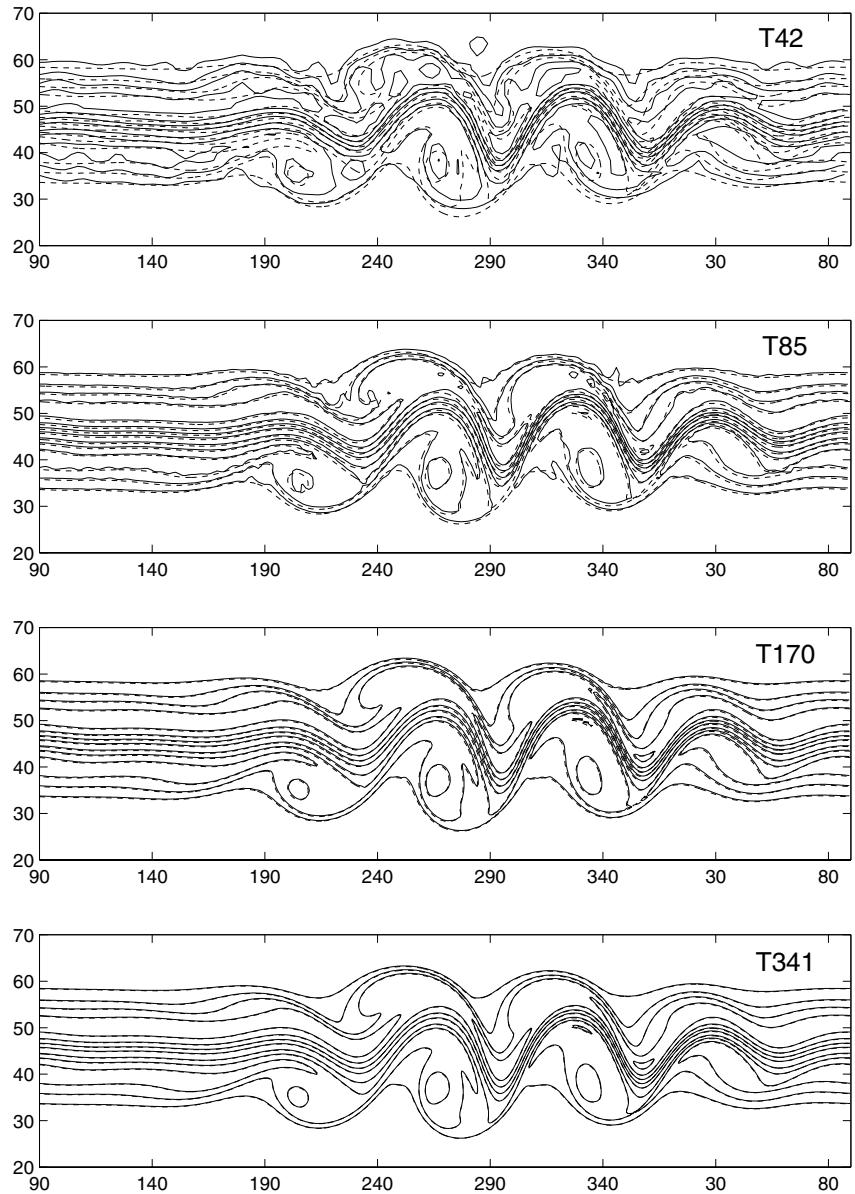
Fig 8. The vorticity field at 144 h for the BOB-SWM solutions at T42, T85, T170 and T341 (solid lines). In each panel, an identical set of dashed lines show the FMS-SWM solution at T341.

the truncation errors associated with some numerical schemes might be sufficiently large to initiate the instability. In order to proceed to the next step, the resolution must be sufficiently refined so that truncation errors do not initiate the barotropic instability.

Secondly, add the perturbation to the height field as given in eq. (4), and integrate for 6 h to numerical convergence, again with no diffusion. The height and divergence fields at 2, 4 and 6 h should closely match those in Fig. 2. Furthermore, we offer in Table 1 a short list of quantities that we believe should be reproducible with any numerical model. The values in Table 1 were obtained with the FMS-SWM, and validated with the BOB-SWM. For each quantity, we report only those digits that were found to be identical in both models.

Thirdly, add the explicit diffusion terms as shown in eq. (1), with the value $\nu = 1.0 \times 10^5$ m^2 s^{-1}, and integrate to 144 h (6 d). Compare the numerically converged vorticity field with that shown in Fig. 6. We believe that even the smaller features in this figure can be reproduced, as the diffusion controls the smallest scales. This can be confirmed by direct comparison of the contour plots. In Table 1, we offer a few quantities relating to the vorticity field at 144 h. Again, these values were computed with two different models and should be easily reproducible.

In conclusion, the test case presented in this paper is only a small step. Its main value is that the solutions computed here are easily reproducible, and that the associated flows are representative of the complexity of the Earth's atmosphere. The next step toward an objective comparison of different numerical schemes
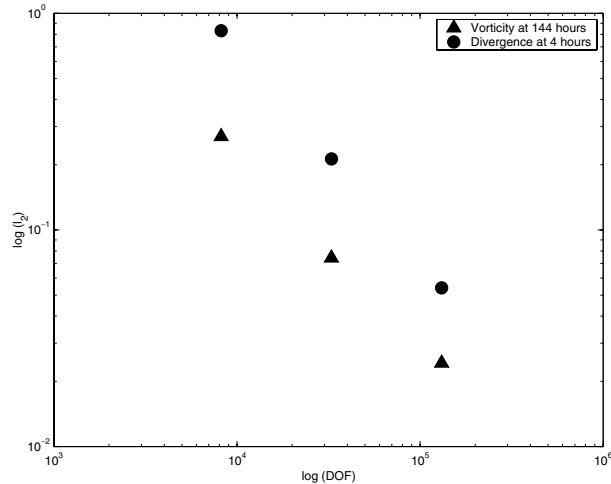
Fig 9. Log–log plot of relative error norms for the BOB-SWM solutions relative to the FMS-SWM solutions at T341, as a function of the number of degrees of freedom of the BOB-SWM solutions. Circles represent $l_2(\delta)$ at 4 h, and triangles $l_2(\zeta)$ at 144 h. The three pairs of points correspond, from left to right, to the T42, T85 and T170 BOB-SWM solutions, respectively.

Table 1. Some reference values of the computed fields for the solutions of the new test case, at the initial adjustment stage ($t = 4$ h), and at the later vorticity roll-up stage ($t = 144$ h)

	Value
At $t = 4$ h	
$l_2(\delta)$	4.0×10^{-7} s^{-1}
max(δ)	3.7×10^{-6} s^{-1}
min(δ)	-2.0×10^{-6} s^{-1}
$l2(h)$	9778 m
max(h)	10 182 m
min(h)	9052 m
At $t = 144$ h	
$l_2(\zeta)$	2.1×10^{-5} s^{-1}
max(ζ)	9.3×10^{-5} s^{-1}
min(ζ)	-7.3×10^{-5} s^{-1}

would involve designing a set of diagnostics for quantitatively assessing accuracy, speed, ease of implementation, and other issues. All of these are, of course, well beyond the scope of the present paper.

References

Baines, P. G. 1976. The stability of planetary waves on a sphere. *J. Fluid Mech.* **73**, 193–213.

Dritschel, D. G., Polvani, L. M. and Mohebalhojeh, A. R. 1999. The contour-advective semi-Lagrangian algorithm for the shallow-water equations. *Mon. Weather Rev.* **127**, 1551–1565.

Hoskins, B. J. and Simmons, A. J. 1975. Multilayer spectral model and semi-implicit method. *Q. J. R. Meteorol. Soc.* **119**, 637–655.

Jakob-Chien, R., Hack, J. J. and Williamson, D. L. 1995. Spectral transform solutions to the shallow-water test set. *J. Comput. Phys.* **119**, 164–187 (J95).

Kiehl, J. T., Hack, J., Bonan, G., Boville, B. and Briegleb, B.. 1996. Description of the NCAR Community Climate Model (CCM3). NCAR Technical Note NCAR/TN-420+STR.

Kuo, A. and Polvani, L. M. 1997. Time-dependent fully nonlinear geostrophic adjustment. *J. Phys. Ocean.* **27**, 1614–1634.

Polvani, L. M., Scott, R. K. and Thomas, S. J. 2004. Numerically converged solutions of the global primitive equations for testing the dynamical core of atmospheric GCMs. *Mon. Wea. Rev.* in press.

Rivier, L., Loft, R. and Polvani, L. M. 2002. An efficient spectral dynamical core for distributed memory computers. *Mon. Wea. Rev.* **130**, 1384–1396.

Scott, R. K., Rivier, L. G., Loft, R. D. and Polvani, L. M. 2004. BOB, model description and user's guide. NCAR Technical Note NCAR/TN-404+IA.

Thuburn, J. and Li, Y. 2000. Numerical simulations of Rossby–Haurwitz waves. *Tellus* **52A**, 181–189.

Williamson, D. L., Drake, J. B., Hack, J. J., Jakob, R. and Swarztrauber, P. N. 1992. A standard test set for numerical approximations to the shallow water equations in spherical geometry. *J. Comput. Phys.* **102**, 211–224 (W92).